*Invited Paper*

# All-silicon terahertz metamaterials absorber and pesticides sensing

Zijian Cui, Yue Wang *, Xiang Zhang, Yongqiang Zhu, and Dachi Zhang
Key Laboratory of Ultrafast Photoelectric Technology and Terahertz Science in Shaanxi, Xi'an University of Technology, 710048, Xi'an, Shaanxi, China
* Email: wangyue2017@xaut.edu.cn

(Received June 2021)

**Abstract**: Perfect absorption based on metamaterials at terahertz frequencies range has attracted a great deal of interest in the field of sensing, imaging, bolometers and stealth technology. This review is focused on presenting several recently developed absorbers based on all-silicon metamaterials, such as single-band, dual-band, multi-band and broadband absorbers. The partial physical mechanisms and optical tunability corresponding to the absorption are also reported. Furthermore, the presented absorbers can be used to detect the concentration of trace pesticides, and a good linear regression coefficient was obtained between the absorption amplitude and the concentration. Notably, the presented all-silicon metamaterials perfect absorbers are compatible with COMS processing which is beneficial to promote the development of terahertz functional devices.

**Keywords**: Terahertz absorber, Metamaterials, Sensing, All-silicon

**doi: 10.1051/tst/2021142031**

## 1. Introduction

Metamaterial is artificial material with periodical arrangement of unit resonator, which has attracted considerable research interest in the past few decades [1-5]. Perfect metamaterial absorber in terahertz (THz) range is an important research topic to explore the potential of this special frequency region, and has become an effective means to fill the "THz gap" in the electromagnetic spectrum [6-8]. Such metamaterials can achieve resonance with the incident electromagnetic over a designed frequency region and match the impedance of the free-space, and therefore, implementing a near-unit absorption property [9, 10]. Perfect metamaterial absorbers in THz frequency have exploited advances in the application fields of stealth coating, detection, filter, and biosensing [11-14].

At present, most metamaterial absorbers use a multi-layer metal-silicon structure with a metal ground to suppress transmission [15]. On account of the difficulty in adjusting the electrical properties of the metal, the tunability corresponding to the absorption are inhibited. Although the

tunability of the devices can be achieved by introducing micro-electromechanical systems or by adding active materials in the unit cell, it is difficult to be realized without the addition of elements with special function. Due to the influence of the photoexcitation on the carriers in silicon, the design of metamaterial absorbers using all-silicon materials with semiconductor properties becomes a window opened on flexible manipulation of absorption characteristics [16-18].

In this paper, we will introduce a series of works on all-silicon terahertz metamaterials absorber carried out by our research group, including the device design, absorption mechanism, tunable characteristics under optical-pump THz-probe (OPTP). It contains diverse kinds of metamaterial absorber designs exhibiting different resonance properties, such as single-band, multi-band, broadband all-silicon absorbers. Meanwhile, a more accurate optical pumping model is established, which can more accurately describe the effect of optical excitation on the dielectric properties of the silicon unit cell. In addition, we have investigated the application of all-silicon terahertz metamaterials absorber in the analyte sensing and trace amount of pesticide detection. The analysis and research of all-silicon metamaterials have enriched the design strategy of metamaterials devices and their application value, and brought new development for implementation of tunable metamaterial and new-type detection techniques.

## 2. THz All-silicon metamaterials absorber

As one of the most important types of terahertz metamaterial absorbers, a series of all-silicon absorbers with different resonance properties have been developed. A variety of absorption characteristics, such as single narrow band, multi-band, and broadband absorption, have been realized, showing the considerable potential in different application scenarios.

### *2.1 Single narrow band absorber*

Due to the complexity of the response of the silicon-based unit cell and the dispersion characteristics of silicon, it is often difficult to implement single-band metamaterial absorbers using silicon-based materials. We have implemented an improved cylindrically shaped periodical single narrow band absorber based on p-type doped silicon [19]. Schematic of designed THz plasmonic metamaterial absorbers (PMAs) of the designed PMAs is shown in Fig. 1(a) and 1(b).

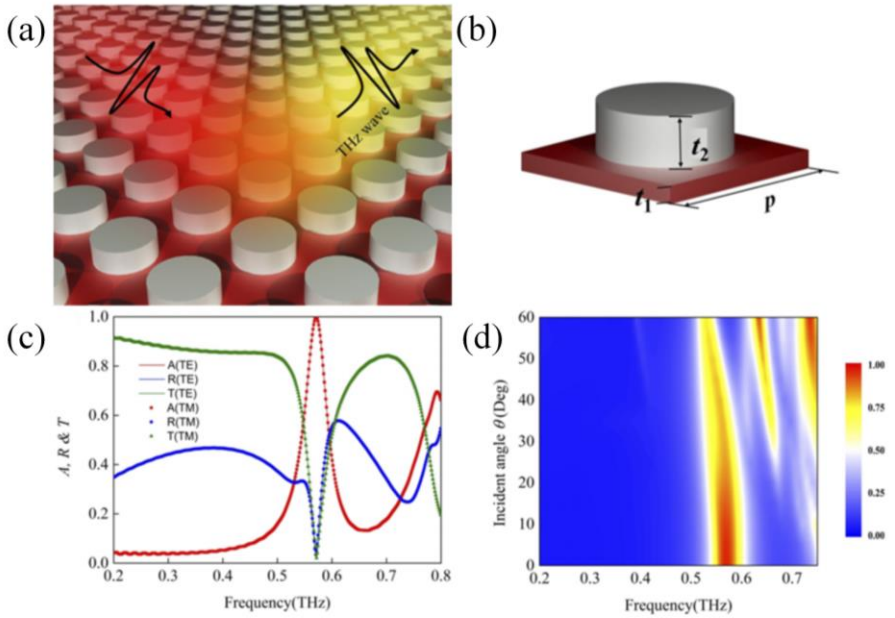


Fig. 1 (a) Schematic of all-silicon THz plasmonic metamaterial absorbers (PMAs). (b) SEM image of the designed PMAs. (c) Transmission (T), reflection (R) and absorption (a) spectra of normal incidence TE and TM modes, and (d) different incidence angles $\theta$ The absorption spectrum of the absorber [19].

We have used different doped silicon carrier densities and polyimide substrate and achieved a higher quality factor (Q) and a large modulation depth of the absorption. The designed device operates in the frequency range of about 0.5-0.6 *THz*. When the absorption value of even mode and odd mode is 0.5 and the radiation loss is equal to the material loss, the perfect absorption can be obtained. On account of the symmetry of the structure, the absorption is insensitive to TE and TM modes incident and the absorption peaks of the two polarization states remain above 70% in the range of 50 °incident angle, as shown in Fig. 1 (c) and (d), and the absorption amount is close to 99.75%. The results show that the calculated Q value and modulation depth (65.31%) has been improved compared with the existing works [20].

*2.2 Dual-band absorber*

By adjusting the coupling between different modes, the absorption of the THz all-silicon metamaterial absorber can be split into two bands. We have proposed a THz all-silicon metamaterial absorber, which can achieve dual-band absorption characteristics [21]. The unit cell of THz all-silicon metamaterial absorber is shown in Fig. 2(a), which is composed of a cylinder and a ring pillar. The experimental results (solid green curve) and simulation results of dual-band THz all-silicon metamaterial absorber are shown in Fig. 2(b). The absorption spectrum consists of two discrete peaks at 0.97 and 1.93 *THz*, respectively. Each of the absorption peaks has more than 99.6% absorption.

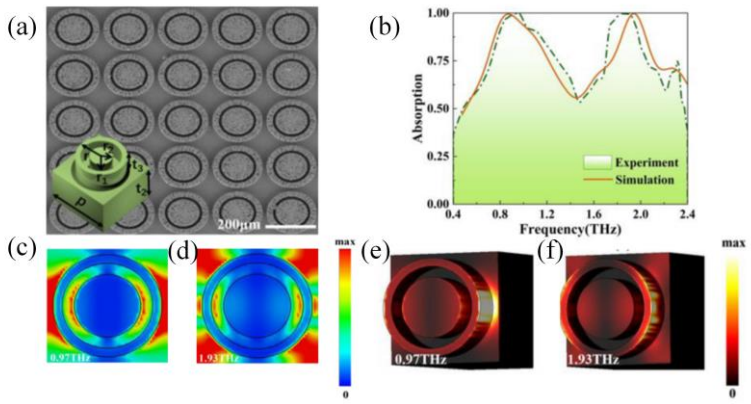


Fig. 2 (a) SEM image of dual frequency sample. Inset: unit cell geometry of the dual-band THz all-silicon metamaterial absorber. (b) Absorption characteristics of simulated (orange curve) and measured (green part) of dual-band. Electric field distribution for (c) 0.97 *THz* and (d) 1.93 *THz* of the dual-band absorber. Power loss density for (e) 0.97 *THz* and (f) 1.93 *THz* of the dual-band absorber [21].

As shown in Fig. 2(c), the electric field distribution of the dual-band THz all-silicon metamaterial absorber at 0.97 *THz* shows that the electric field is concentrated in the gap between the two sides of the cell and the ring and cylinder. This distribution is caused by the dipole resonance which enhances the plasma effect. At the 1.93 *THz*, the second resonance peak occurs, due to the coupling of higher-order modes, and the electric field is widely distributed on the left and right sides of the structure, as shown in Fig. 2(d). The low frequency absorption peak is the fundamental resonance of the structure, and the high frequency absorption peak comes from the inherent electric resonance. For the dual-band THz all-silicon metamaterial absorber, most of the power is dissipated in the metamaterial layer, as shown in Fig. 2(e) and 2(f).

### *2.3 Multi-band absorber*

Absorbers with more absorption bands have unique advantages in some special applications, such as sensing. A metamaterial absorber based on the silicon grating which can achieve quad-band or tri-band perfect absorption in the THz regime is designed [22]. The structure design of perfect metamaterial absorber is based on one-dimensional all-silicon grating, which is made of N-doped silicon. The maximum and minimum absorptivity of the quad-band absorber are 98.03% and 91%, respectively. Similarly, the maximum absorption of the tri-band absorbent is 99.99%, and the minimum absorption is more than 91%. The maximum Q of quad-band and tri-band absorber are 12.64 and 12.46, respectively. The quad-band and tri-band absorbers are composed of the same structure, but the etching depth is slightly different.

The quad-band absorber has four strong resonance absorption peaks, and the grating height $d$ = 108 $\mu m$. At the resonant frequencies of about 0.49, 1.05, 1.73 and 2.04 *THz*, the peak absorption amplitude is more than 90%, and the absorption efficiency is 91.79%, 95.95%, 97.89%, and 98.03%, respectively. The tri-band absorber has three strong resonance absorption peaks, and the

grating height $d$ = 160 $\mu m$. Three resonance absorption peaks are at about 0.36, 1.37 and 2.18 *THz*. The peak absorption amplitudes are to 91.50%, 97.55% and 99.99%, respectively.

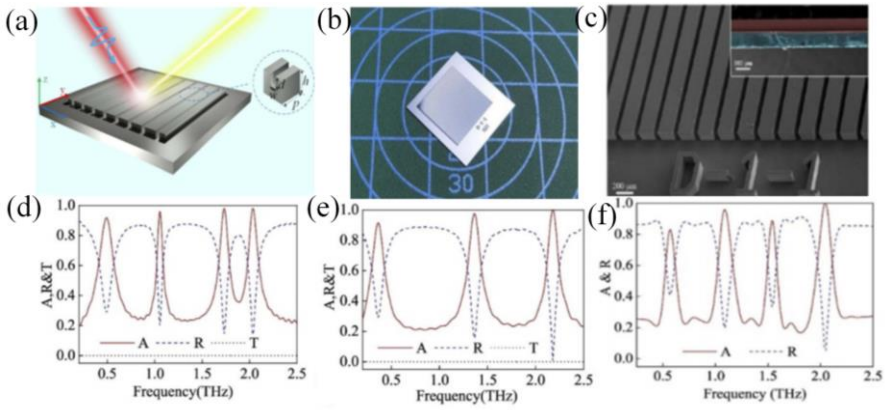


Fig. 3 (a) Schematic of all-silicon THz plasmonic metamaterial absorbers (PMAs). (b) Physical photograph of the PMAs. (c) SEM image of the designed PMAs. Inset: false color scanning electron micrograph of the lateral wall of the structure. The red part is the etched silicon, and the blue part is the silicon substrate. (e), (f) The absorption spectra of quad-band (e) and tri-band (d) PMAs, respectively. (f) The absorbance and reflectance spectrum of the fabricated absorber with experiment [22].

### *2.4 Broadband absorber*

Broadband absorbers are more suitable for broadband applications, such as stealth coating. Herein, a broadband PMAs based on all silicon split ring resonators which use a simple design on highly n-type doped silicon is designed and demonstrated by experiments [23]. The schematic diagram and the SEM image of PMA structure are shown in Fig. 4(a) and 4(b). As shown in Fig. 4(c), the broadband absorber is able to reach more than 90% absorption in the range from 0.95 to 2.0 *THz*. And three resonant peaks with nearly 100% absorption are at 1.03, 1.45, and 1.77 *THz*.

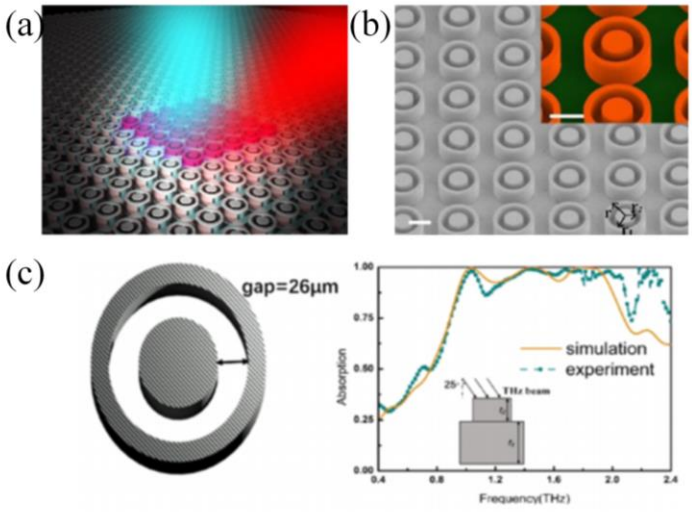


Fig. 4 (a) Schematic of all-silicon THz PMAs. (b) SEM image of the designed PMAs. (c) Illustrations of unit cells of SRRs and simulated (yellow curve) and measured (green curve) absorption characteristics of the broadband PMAs [23].

From a macroscopic point of view, the metamaterial layer on the silicon substrate realizes the function of reducing reflection coating. Coupling between the multiple modes results in a broadband absorption characteristic that maintains a high absorption rate over a wide frequency range.

## 3. Dynamic behavior under photoexcitation

Due to the effect of the photoexcitation on the carriers in silicon, the design of metamaterial absorbers using all-silicon materials behave as tunable devices. In this section, we will discuss optical tunability of the terahertz all-silicon metamaterials absorber based on our previous work [24].

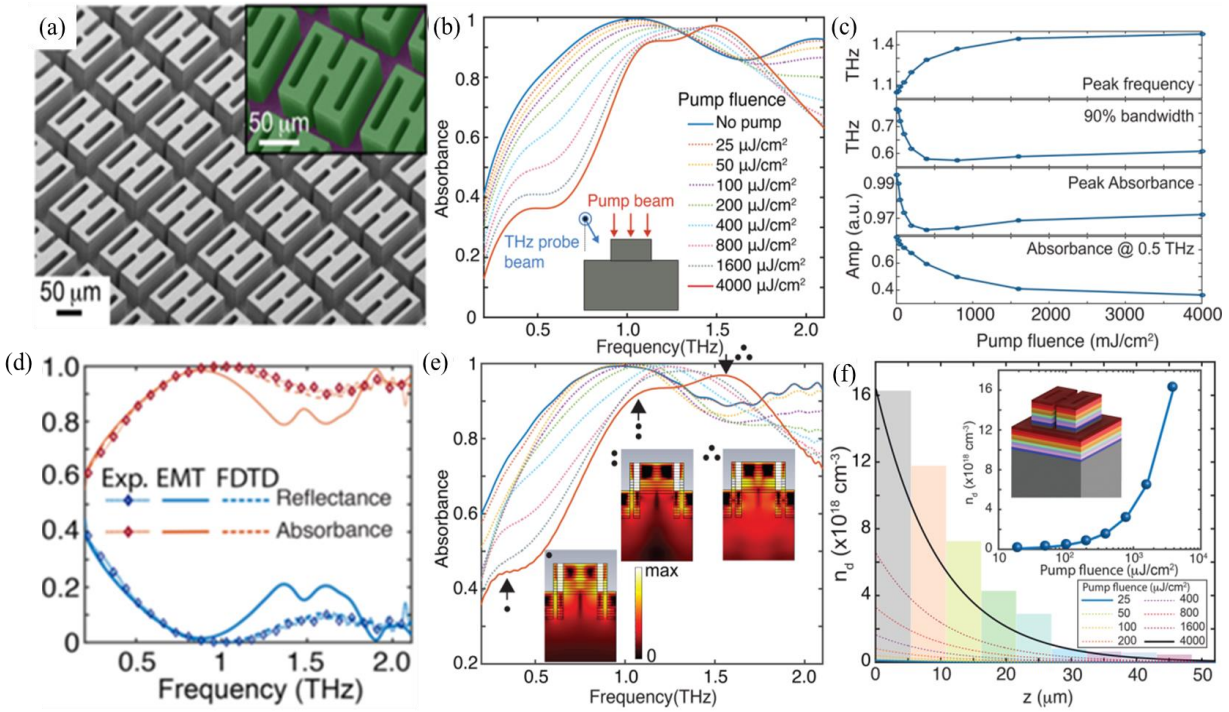


Fig. 5 (a) Scanning electron microscope (SEM) image of the all-silicon metamaterial absorber. Inset: false color SEM view of the unit cell. (b) optically pumped terahertz probe spectrum of the all-silicon metamaterial absorber for different pump fluences. Inset: incident direction of the beams; the optical pump beam is at normal incidence and the THz probe beam is at 30 °angle of incidence. (c) The peak absorption frequency, bandwidth, peak absorbance amplitude and absorbance at 0.5 *THz*. (d) experimental and simulation results (e) Simulation results with layered carrier density distribution to match the measured spectrum for different pump fluences in (b). Insets: the power loss density distribution for each resonant mode. (f) The theoretically calculated carrier density distribution along the z-axis in the all-silicon metamaterial absorber for different pump fluences. The bar plot represents the carrier density for each slice used in the simulation to match the spectrum for the maximum pump fluence [24].

We have analyzed the carrier dynamics caused by the optical pump to explain the physical principles behind the tunable phenomenon, and have compared the simulated absorption spec-

trum with the experimental results. Firstly, we consider a homogeneous increase in the carrier densities in the silicon (metamaterial layer and substrate) induced by the optical excitation. However, the simulated results fail to capture the resonance peaks, indicating that modeling the carrier concentration as homogeneous is inaccurate. Therefore, we consider nonuniformity in the distribution of carrier density. According to the Beer-Lambert law, for the 800 *nm* pump beam, the fluency decays exponentially along the propagation direction, with $f(z) = f_0 e^{-az}$, where $f_0$ is the fluence at the top surface of the silicon structure ($z = 0$), $a$ ($\approx 1020\ cm^{-1}$) is the absorption coefficient for the pump beam and $z$ is the depth in the silicon. We assume that all of the absorbed photons are converted to carriers in the silicon. The carrier density distribution in silicon along $z$ direction can be estimated by [25]:

$$n_d(z) = \frac{1}{E_{photon}} \cdot \frac{df(z)}{dz} = \frac{\alpha f_0 e^{-\alpha z}}{E_{photon}} \tag{1}$$

where $E_{photon}$ ($=h\nu$) is the photon energy of the pump beam, $h$ is Planck's constant, and $\nu$ is the frequency of the pump beam. The carrier density ($n_d$) distribution is shown in Fig. 5(f) for different pump fluences, indicating that the maximum carrier density is achieved at the top surface and decays exponentially into the surface. The carrier density at the top surface of silicon is related linearly to the pump fluence, as shown in the inset of Fig. 5(f), and the maximum carrier density is approximately $16 \times 10^{18}\ cm^{-3}$ for the maximum pump fluence (i.e., 4000 $\mu J/cm^2$), which is of the same order as previously reported value [25, 26]. The analysis of carrier density distribution indicates that we are unable to excite the all-silicon metamaterial absorber structure homogeneously using the pump beam. Because the thickness of the metamaterial layer is too large, we need to further consider the carrier density gradient in our simulation. However, it is difficult to include spatially distributed carrier densities in the numerical simulation. So, we need to slice the metamaterial layer, as shown in the inset of (Fig. 5f). Therefore, we divide the metamaterial layer with a height of 53 $\mu m$ into 10 pieces, each with a thickness of 5.3 $\mu m$, and approximate the different carrier density in each slice to model the gradient distribution of the carrier density.

In the simulation, we set the top two layers with a carrier density of $0.1 \times 10^{18}\ cm^{-3}$, but the other slices are without any changes to fit the measured absorbance under 25 $\mu J/cm^2$, as shown in Fig. 5(e). As the pump fluence increases, we observe that the absorbance spectrum shift is similar to the experimental results. In the experiment, we used the OPTP spectroscopy to study the tunable response of the all-silicon metamaterial absorber under optical excitation. The THz beam is at a 30° angle of incidence and the optical pump beam is normally incident. The pump beam is 800 *nm* near-infrared light with pulse duration of 35 *fs*, which arrives at the sample 10 *ps* prior to the THz probe beam to ensure quasi-equilibrium of the electrons excited into the conduction band. Fig. 5(b) shows the OPTP spectra of the all-silicon metamaterial perfect absorber. When there is no pump beam, the spectrum is similar to the Fig. 5(d). The results we get are that the peak absorption frequency is approximately 1.04 *THz* with bandwidth of 770 *GHz*. As the fluence of the pump beam increases to 4000 $\mu J/cm^2$, the peak absorption frequency has blueshift to 1.48 *THz*

due to photoexcitation of carriers in silicon. At the same time, the bandwidth of 90% absorption decreases to 600 *GHz* and the absorption coefficient decreases from 99.6% to 97.2%, as shown in Fig. 5(c). When the fluence is higher than 400 $\mu J/cm^2$, weak resonances move from 0.45 *THz* to 0.92 *THz*, indicating new modes present in the pumped condition. The absorbance at 0.5 *THz* is modulated from 80% to 36%.

## 4. Sensing applications of trace amount of pesticide

Analyte sensing is one of the most important examples of terahertz metamaterial absorber applications, because sensing applications mediated by metamaterial absorber are extremely convenient and nondestructive. Due to strong local field enhancement, the effects of trace amount of analytes are amplified for sensing applications under very few conditions. With the employment of simulation as well as experiment, the analyte simulation and detection can be suitably used to display the sensing properties of THz metamaterial applications.

### *4.1 Simulation study of metamaterial absorber sensing applications*

The properties of all-silicon THz metamaterial absorber make it able to absorb electromagnetic waves well, and it has a wide range of applications as an absorber. For example, they can be used as an absorber unit for biological Terahertz sensor. Here, we investigate a periodic single narrow-band absorber consisting of a square polyimide substrate and a cylindrical p-doped silicon array, as shown in the inset of Fig. 6(a). [19]. The absorber demonstrates perfect absorption at 0.57 *THz* with an absorbance close to 99.75% and a Q of 11.278. And, we simulate the relationship between the absorption of the absorber and the thickness of the specimen. From Fig. 6(b), it can be seen that there is a slight red shift of the peak absorbance with increasing thickness. Fig. 6(b) shows the absorption change caused by the refractive index change at a certain thickness. The results show that there is also a slight red shift of the absorption peak with increasing refractive index. In Fig. 6(c) and 6(d), we can observe the changes of absorption frequency and frequency peaks more visually. This work demonstrates the feasibility of the prepared absorber for sensing applications and also provides a new design idea for practical applications of terahertz all-silicon metamaterials.

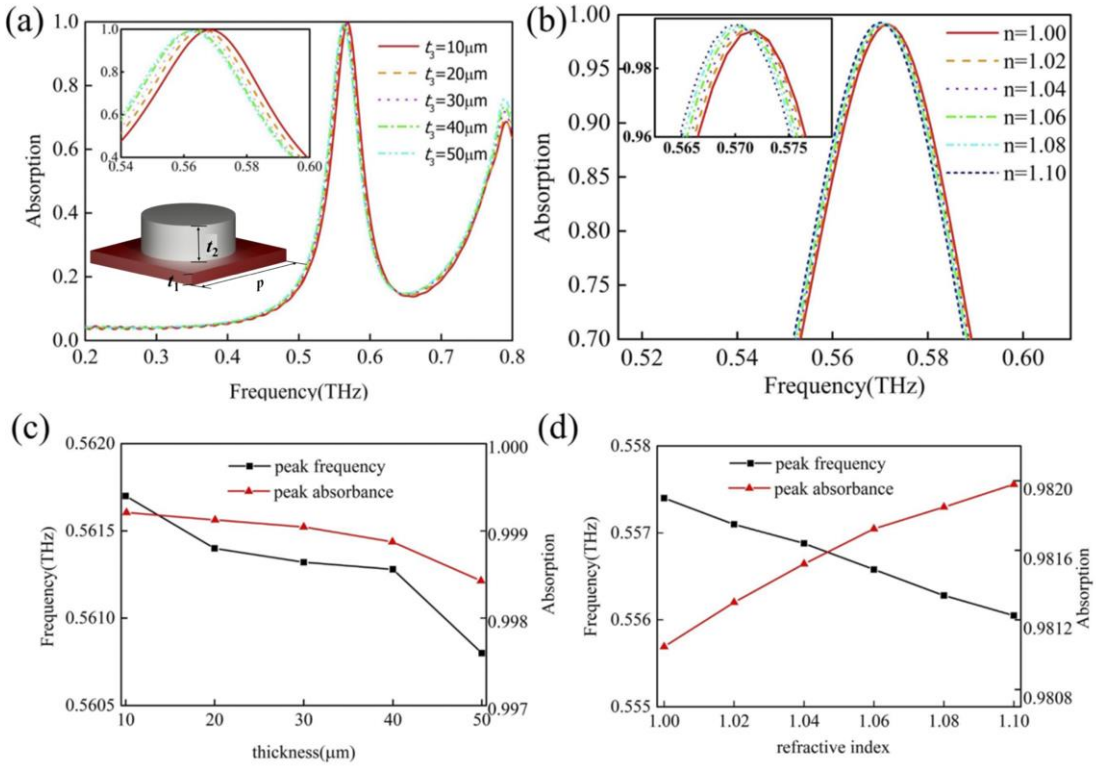


Fig. 6 (a) Describes the absorption for different refractive indexes with the same sample thickness, (b) describes the absorption at different thicknesses with the same sample refractive index, (c) describes the change in the absorption frequency and frequency peak as the thickness increased, and (d) describes the change in absorption frequency and frequency peak as the refractive index increased [19].

### *4.2 Metamaterial absorber for 2,4-D detection applications*

As mentioned above, because all-silicon THz metamaterial absorber depends on the refractive index of the surrounding environment, it is verified that an all-silicon THz metamaterial absorber can be used as biosensors in terahertz systems as a good candidate. We fabricate all-silicon THz metamaterial absorber on n-type doped silicon by conventional photolithography and deep reactive ion etching [21]. The unit with single band absorber structure is shown in Fig. 7(a), which is composed of a silicon surface array on which the structure is etched. As shown in Fig. 7(b), a significant change in the absorption spectrum of the device can be found when the 2, 4-D solution is added on the surface of all-silicon THz metamaterial absorber. For 2, 4-D concentrations from 0.05 to 4 *ppm*, the amplitude of the absorption peak increases with increasing 2, 4-D concentration. We attribute this increase in the amplitude of the absorption peak to the behavior of the anti-reflective coating, which reduces the surface reflection and thus leads to an increase in absorption.

Further researches show that a good linear relationship between the concentration and absorption intensity of 2, 4-D has been achieved, as shown in Fig. 7(c). The regression coefficient between absorption intensity and concentration can reach 0.9429. The orange dots indicate the av-

erage of the five sets of absorption peak amplitudes and the error bars caused by the internal instability of the THz-TDS system. To verify the reliability of the terahertz sensor, the pesticide concentration of 1 *ppm* is tested separately and the results are shown in the pentagram position in Fig. 7(c), which confirms the feasibility of the proposed terahertz sensor with an all-silicon metamaterial.

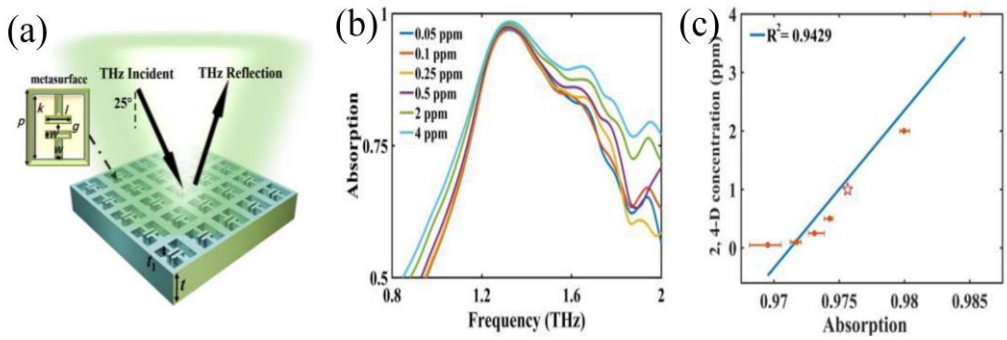


Fig. 7 (a) Illustration of the single-band THz all-silicon metamaterial absorber and the inset plot shows the unit cell geometry of the design. (b) Measured absorption spectra of the single-band THz all-silicon metamaterial absorber for 0.05– 4 *ppm* of 2, 4-D. (c) Regression curves established for the single-band THz all-silicon metamaterial absorber based on spectral intensity variations [21].

### *4.3 Metamaterial absorber for chlorpyrifos detection applications*

Chlorpyrifos is a highly effective and broad-spectrum organophosphorus pesticide. It has the triple effects of stomach toxicity, touch killing and fumigation, and is a moderately toxic pesticide. It is widely used to control many fruit and vegetable pests, as well as a variety of underground pests. However, overuse of chlorpyrifos has resulted in residues of this drug in food, which poses a risk of adverse health effects to consumers. Here, we have investigated a highly sensitive method using THz-TDS in combination with a pre-designed metamaterial absorber for the detection of chlorpyrifos [27]. As shown in Fig. 8(a) metamaterial absorber consisting of a coaxial ring and a cylinder etched on a doped silicon wafer. In the experiments, we drop samples with different concentrations of chlorpyrifos solution on the surface of the metamaterial absorber and dry them. The average absorption spectra of the metamaterial absorber in the presence and absence of chlorpyrifos solution are shown in Fig. 8(b). When chlorpyrifos solution is added to the surface of the absorber, the dielectric properties of the absorber are changed by chlorpyrifos in the grating, and the THz absorption Spectrum of the absorber is changed obviously. As shown in Fig. 8(c) and 8(d), a good linear relationship between chlorpyrifos concentration and absorption intensity values as well as resonance frequency shift. The regression coefficients of chlorpyrifos concentration with peak intensity and frequency shift are 0.9943 and 0.9750, respectively. The results show that the peak intensity and frequency shift of the spectrum resonate well with the concentration of chlorpyrifos in the range of 0.1 ~ 100 $mg \cdot L^{-1}$ when the surface of all-silicon metamaterial is covered with chlorpyrifos residue. In conclusion, the proposed all-silicon terahertz metamaterial absorber can be used as a fast and accurate sensing tool for the

determination of trace substances, which provides a new and reliable idea for various applications of biological science.

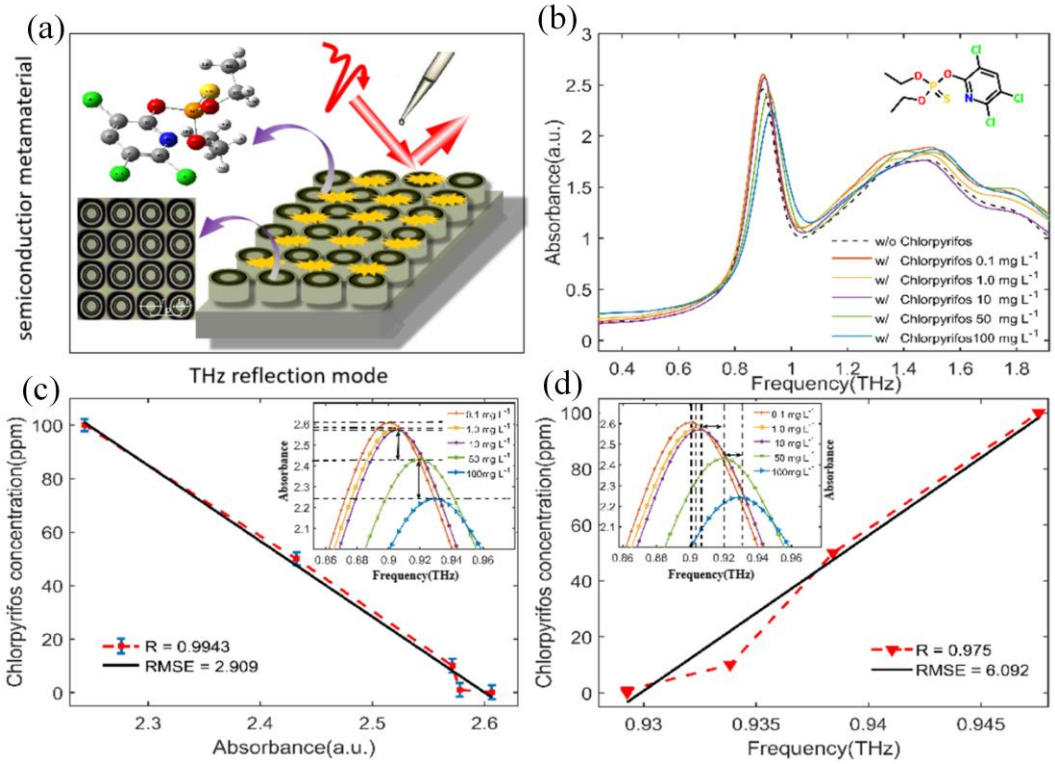


Fig. 8 (a) Schematic diagram of chlorpyrifos detection by terahertz metamaterial. (b) The measured absorption spectra of chlorpyrifos containing and chlorpyrifos free metamaterials. (c) The regression curve of spectral intensity changes and (d) frequency shift was established [27].

## 5. Conclusions

The strong local resonance of the incident THz wave at the unit cell of the metamaterial absorber produces near-unit absorption characteristics. Due to the adoption of silicon in the structure, the absorption characteristics of all-silicon THz metamaterial absorber can be manipulated flexibly by adjusting the pump light. In addition, their linear response to the pesticide concentrations also shows great potential in the field of the detection of trace amount of pesticide residue. Further research with all-silicon THz metamaterial absorber is also of significance, especially in combination with other advanced application fields, such as specific biological nondestructive detection.

## Acknowledgment

This work was supported in part by the Youth Innovation Team of Shaanxi Universities under Grant 21JP084, and in part by the National Natural Science Foundational of China under Grant

61975163, and in part by the Natural Science Foundation of Shaanxi Province under Grant 2020JZ-48，and in part by Open Project of Key Laboratory of Engineering Dielectrics and Its Applications (Harbin University of Science and Technology), Ministry of Education under Grant KEY1805.

## References

[1] J. Zhu, Z. Ma, W. Sun, et al.. "Ultra-Broadband Terahertz Metamaterial Absorber". *Appl. Phys. Lett.*, 105, 021102 (2014).

[2] B. Wang, L. Wang, G. Wang, et al.. "Frequency Continuous Tunable Terahertz Metamaterial Absorber". *J. Lightwave Technol.*, 32, 1183-1189 (2014).

[3] G. Duan, J. Schalch, X. Zhao, et al.. "An Air-Spaced Terahertz Metamaterial Perfect Absorber". *Sens. Actuator A-Phys.*, 280, 303-308 (2018).

[4] M. Pu, M. Wang, C. Hu, et al.. "Engineering Heavily Doped Silicon for Broadband Absorber in the Terahertz Regime". *Opt. Express*, 20, 25513-25519 (2012).

[5] X. Duan, S. Chen, W. Liu, et al.. "Polarization-Insensitive and Wide-Angle Broadband Nearly Perfect Absorber by Tunable Planar Metamaterials in the Visible Regime". *J. of Opt.*, 16, 125107 (2014).

[6] F. Hu, T. Zou, B. Quan, et al.. "Polarization-Dependent Terahertz Metamaterial Absorber with High Absorption in Two Orthogonal Directions". *Opt. Commun.*, 332, 321-326 (2014).

[7] G. Wang, and B. Wang. "Five-Band Terahertz Metamaterial Absorber Based on a Four-Gap Comb Resonator". *J. Lightwave Technol.*, 33, 5151-5156 (2015).

[8] J. Schalch, G. Duan, X. Zhao, et al.. "Terahertz Metamaterial Perfect Absorber with Continuously Tunable Air Spacer Layer". *Appl. Phys. Lett.*, 113, 061113 (2018).

[9] Y. Cheng, W. Withayachumnankul, A. Upadhyay, et al.. "Ultrabroadband Plasmonic Absorber for Terahertz Waves". *Adv. Opt. Mater.*, 3, 376-380 (2015).

[10] C. Shi, X. F. Zang, L. Chen, et al.. "Compact Broadband Terahertz Perfect Absorber Based on Multi-Interference and Diffraction Effects". *IEEE Trans. Terahertz Sci. Technol.*, 6, 40-44 (2016)

[11] X. Liu, K. Fan, I. V. Shadrivov, et al.. "Experimental Realization of a Terahertz All-Dielectric Metasurface Absorber". *Opt. Express*, 25, 191-201 (2017).

[12] Y. Li, B. An, S. Jiang, et al.. "Plasmonic Induced Triple-Band Absorber for Sensor Application". *Opt. Express*, 23, 17607-17612 (2015).

[13] X. Zang, C. Shi, L. Chen, et al.. "Ultra-Broadband Terahertz Absorption by Exciting the Orthogonal Diffraction in Dumbbell-Shaped Gratings". *Sci. Rep.*, 5, 8901 (2015).

[14] W. Withayachumnankul, C. M. Shah, C. Fumeaux, et al.. "Plasmonic Resonance toward Terahertz Perfect Absorbers". *ACS Photonics*, 1, 625-630 (2014).

[15] M. K. Hedayati, F. Faupel, and M. Elbahri. "Tunable Broadband Plasmonic Perfect Absorber at Visible Fre-

quency". *Appl. Phys. A-Mater. Sci. Process.*, 109, 769-773 (2012).

[16] D. Hashimshony, I. Geltner, G. Cohen, et al.. "Characterization of the Electrical Properties and Thickness of Thin Epitaxial Semiconductor Layers by THz Reflection Spectroscopy". *J. of Appl. Phys.*, 90, 5778-5781 (2001).

[17] C. Shi, X. Zang, Y. Wang, et al.. "A Polarization-Independent Broadband Terahertz Absorber". *Appl. Phys. Lett.*, 105, 031104 (2014).

[18] W. Withayachumnankul, C. M. Shah, C. Fumeaux, et al.. "Terahertz Localized Surface Plasmon Resonances in Coaxial Microcavities," *Adv. Opt.l Mater.*, 1, 443-448 (2013).

[19] Y. Wang, L. Yue, Z. Cui, et al.. "Optically tunable single narrow band all-dielectric terahertz metamaterials absorber". *AIP Adv.*, 10, 045039 (2020).

[20] K. Fan, J. Zhang, X. Liu, et al.. "Phototunable Dielectric Huygens' Metasurfaces". *Adv. Mater.*, 30, 1800278 (2018).

[21] Y. Wang, D. Zhu, Z. Cui, et al.. "Properties and Sensing Performance of All-Dielectric Metasurface THz Absorbers". *IEEE Trans. Terahertz Sci. Technol.*, 10, 599-605 (2020).

[22] L. Yue, Y. Wang, Z. Cui, et al.. "Multi-band terahertz resonant absorption based on an all-dielectric grating metasurface for chlorpyrifos sensing". *Opt. Express*, 29, 13563-13575 (2021).

[23] Y. Wang, D. Zhu, Z. Cui, et al.. "All-dielectric terahertz plasmonic metamaterial absorbers and high-sensitivity sensing". *ACS omega*, 4, 18645-18652 (2019).

[24] X. Zhao, Y. Wang, J. Schalch, et al.. "Optically Modulated Ultra-Broadband All-Silicon Metamaterial Terahertz Absorbers". *ACS Photonics*, 6, 830-837 (2019).

[25] A. Sabbah, and D. M. Riffe. "Femtosecond Pump-Probe Reflectivity Study of Silicon Carrier Dynamics". *Phys. Rev. B*, 66, 165217-165228 (2002).

[26] K. Fan, J. Zhang, X. Liu, et al.. "Phototunable Dielectric Huygens' Metasurfaces". *Adv. Mater.*, 30, e1800278 (2018).

[27] P. Nie, D. Zhu, Z. Cui, et al.. "Sensitive detection of chlorpyrifos pesticide using an all-dielectric broadband terahertz metamaterial absorber". *Sens. Actuator B-Chem.*, 307, 127642 (2020).